Isoelectronic x-ray spectroscopy to determine electron temperatures in long-scale-length inertial-confinement-fusion plasmas

T. D. Shepard, C. A. Back, D. H. Kalantar, R. L. Kauffman, C. J. Keane, D. E. Klem, B. F. Lasinski, B. J. MacGowan, L. V. Powers, L. J. Suter, and R. E. Turner
Lawrence Livermore National Laboratory, P.O. Box 808, Livermore, California 94551-0808

B. H. Failor
Physics International, 2700 Merced Street, San Leandro, California 94577

W. W. Hsing
Los Alamos National Laboratory, P.O. Box 1663, Los Alamos, New Mexico 87545
(Received 24 July 1995)

We have successfully employed isoelectronic line ratios to measure the electron temperature in gas-filled *Hohlraum* targets and gas bags shot with the Nova laser. These targets produce millimeter-scale-length plasmas with electron density $N_e \sim 10^{21}$ cm^{-3} and electron temperature $T_e \sim 3$ keV. The *Hohlraum* targets can also produce radiation temperature exceeding 200 eV. Isoelectronic line ratios are well suited to this measurement because they are relatively insensitive to radiation field effects in *Hohlraum* targets, opacity, transients, and variations in electron density compared to conventional line ratios. We survey the properties of isoelectronic line ratios formed from ratios of n-to-1 resonance transitions in heliumlike Cr to the same transitions in Ti and compare with conventional ratios of n-to-1 transitions in hydrogenlike Ti to the corresponding transitions in heliumlike Ti, concentrating on plasma parameter ranges of interest to the Nova experiments. We also consider the same ratios using K and Cl. Atomic kinetics are treated using collisional-radiative models and experimental data are analyzed with the aid of radiation-hydrodynamics calculations. When we apply isoelectronic techniques to the Nova experimental data, we find that the targets have electron temperatures of at least 3 keV. [S1063-651X(96)08505-4]

PACS number(s): 52.70.La, 52.50.Jm, 52.58.Ns

I. INTRODUCTION

Soft-x-ray line-ratio spectroscopy is a useful technique commonly employed for characterization of laser-produced plasmas [1]. Characterization of the bulk plasma conditions in *Hohlraum* targets is important for understanding *Hohlraum* energetics and laser-plasma instabilities, such as stimulated Brillouin scattering and stimulated Raman scattering [2]. Unfortunately, in *Hohlraum* targets, the presence of the intense radiation drive field [3] complicates the application of standard spectroscopic diagnostic techniques [1]. This radiation field can significantly affect the behavior of line intensity ratios (e.g., resonance-to-satellite ratios) normally used to measure electron temperature T_e and electron density N_e [4]. At relatively high electron densities (supercritical for 0.35-μm light, $N_e > 10^{22}$ cm^{-3}) photon-induced effects are small compared to electron collisional effects and the radiation field is less perturbative. However, the presence of strong spectral background emission from the high-Z (typically Au, $Z=79$) *Hohlraum* wall imposes a minimum requirement on the amount of spectral dopant necessary to produce observable emission. Optical depth of the dopant then becomes a serious issue [5].

The relatively long ionization equilibration time at subcritical densities presents an additional challenge. The need to avoid photon-induced transitions leads us to consider emission lines from widely spaced levels such as K-shell transitions (preferably not including satellites, since these involve a weakly bound spectator electron that may be easily photoionized). Ratios between lines of the same ionization stage [e.g., $I(\mathrm{Ly}_\beta)/I(\mathrm{Ly}_\alpha)$, which is not too sensitive to the radiation field] respond quickly to transients, but have poor T_e sensitivity. [In the case of $I(\mathrm{Ly}_\beta)/I(\mathrm{Ly}_\alpha)$, the poor T_e sensitivity is due to the relatively close energy spacing of the $n=2$ and 3 levels.] For parameters typical of *Hohlraum* bulk plasmas, conventional K-shell line-ratio diagnostics sensitive to the H-like to He-like ionization balance [e.g., $I(\mathrm{Ly}_\alpha)/I(\mathrm{He}_\alpha)$, which we refer to generically as an ''inter-ionization-stage'' or ''interstage'' ratio] are only weakly perturbed by the radiation field and have good T_e sensitivity, but require typically several nanoseconds of steady-state plasma to reach their equilibrium values at subcritical densities ($N_e < 10^{22}$ cm^{-3}). Although this requirement seriously compromises the analysis of transient plasmas in *Hohlraum* targets, the strong T_e sensitivity and weak T_r sensitivity of interstage ratios makes it worthwhile to attempt to use them with the aid of fully time-dependent models to treat the transient behavior. We use them as a benchmark for the isoelectronic ratios. Interstage ratios are also heavily used for the diagnosis of implosions, where transient effects are not important because of the much higher density and resulting fast collisional rates [6].

Recently, Marjoribanks *et al.* [7] successfully employed isoelectronic line ratios for the T_e diagnosis of laser-produced plasmas in open geometries. Isoelectronic line ratios are formed using the same spectral line from two different elements. A plasma is formed containing known relative amounts of impurity dopants of slightly different atomic numbers. The isoelectronic line ratios are formed using transitions between identical pairs of electronic configurations

 © 1996 The American Physical Society

for the two elements [e.g., $I(\mathrm{Cr\ He}_\alpha)/I(\mathrm{Ti\ He}_\alpha)$]. Since the same population mechanisms contribute comparably to both line intensities, each intensity will be given to a good approximation by the same function of

$$U_Z=\frac{P_Z}{T_e}=\frac{Z^2E_R}{T_e}, \tag{1}$$

where P_Z is the ionization potential of element Z and E_R is the Rydberg energy. For example, in the Ration model [8,9] used in our calculations, collisional ionization S is determined using an equation by Lotz [10–12]

$$S=2.97\times10^{-6}\,\frac{\xi\sqrt{U_ZE_1(U_Z)}}{Z^3E_R}, \tag{2}$$

where ξ is the number of outer-subshell electrons in the initial ion stage and E_1 is the exponential integral of the first kind. The nontrivial density dependence (e.g., due to stepwise excitation, shown in Fig. 1, below) cancels fairly accurately, resulting in a ratio that depends primarily on T_e. Other dependences and nonideal effects also tend to cancel when the ratio is formed. As indicated by Marjoribanks *et al.* [7], even uncertainties in the atomic physics model tend to cancel for isoelectronic ratios. This cancellation occurs because such errors contribute comparably to the numerator and denominator in the ratio.

A complication with isoelectronic line ratios is that it is necessary to know the relative abundances of the two elements in the dopant sample to avoid introducing significant error in the measurement. In some cases, such as an $I(\mathrm{K})/I(\mathrm{Cl})$ scheme, the ratio of K to Cl abundances is known accurately by stoichiometry if one uses KCl salt as the dopant. In a more general case, such as $I(\mathrm{Cr})/I(\mathrm{Ti})$, it is necessary to measure the relative abundances (e.g., by x-ray fluorescence).

Our calculations indicate that isoelectronic line ratios are sufficiently insensitive to photon-induced effects, opacity, and transients to be used to measure T_e in *Hohlraum* plasmas.

The remainder of this article is organized as follows. We describe the computer modeling codes we used in Sec. II. We survey the properties of isoelectronic line ratios as predicted by collisional-radiative atomic kinetics calculations in Sec. III and present a simple analytic model that shows less sensitivity to modeling uncertainty of dielectronic recombination for isoelectronic than interstage ratios in Sec. IV. In Sec. V we show some example experimental applications of isoelectronic and interstage ratios, using analysis techniques that account for nonideal effects such as transients and spatial gradients in the determination of T_e. Section VI is devoted to a study of the perturbing effects caused by introduction of the spectral impurity in a gas-filled *Hohlraum* target. The summary is in Sec. VII.

II. MODELING TECHNIQUES

To perform atomic kinetics calculations, we used the Ration model [8,9]. Ration calculates K-shell emission for elements with atomic numbers from 6 (C) to 26 (Fe), using detailed atomic levels for H-like, He-like, and Li-like ionization stages, with all other ionization stages including only ground states. Optical-depth effects in the kinetics are treated in the escape-factor approximation. The physical processes included in the Ration model are electron-impact excitation and deexcitation, electron-impact ionization, three-body recombination, autoionization, dielectronic recombination, photoexcitation, spontaneous emission, photoionization, radiative recombination (spontaneous and stimulated), stimulated emission, and continuum lowering. (Some of these processes, e.g., continuum lowering and three-body recombination, are not important for long-scale-length inertial-confinement-fusion plasmas.)

The two atomic kinetics codes we use are called FLY and DSP (Detailed Spectroscopy Postprocessor) [13]. The LASNEX hydrodynamics code [14] provides plasma parameters for input to FLY and DSP. FLY solves the time-dependent rate equations using the Ration model [15] assuming a uniform (slab) plasma with line transfer treated using escape factors. DSP is also time dependent and uses the Ration model, but performs a spatially dependent calculation by postprocessing data from LASNEX, which has two dimensions representing cylindrical symmetry. DSP uses escape factors [16,17] for the kinetics calculation and produces emission and absorption coefficients for each zone in the hydrodynamics simulations. DSP then generates the simulated spectra by formally solving the radiative transfer equation along the desired lines of sight.

III. PROPERTIES OF ISOELECTRONIC LINE RATIOS

For our *Hohlraum* applications, the interstage line ratio is the best conventional line ratio that we have found. In this section, we compare the isoelectronic line ratio with the interstage ratio. The isoelectronic ratio is superior to the interstage ratio in all respects except that (i) the interstage ratio has somewhat stronger sensitivity to T_e and (ii) the isoelectronic line ratio requires knowledge of the relative concentrations of the two dopants.

Figures 1–4 compare isoelectronic and interstage [18] line ratios, including $I(\mathrm{Ti})/I(\mathrm{Cr})$ and $I(\mathrm{K})/I(\mathrm{Cl})$ schemes that we use for measurements of the gas-filled targets. We have investigated the behavior of a variety of different line ratios for elements with atomic numbers from 12 (Mg) to 26 (Fe). Here we concentrate on ratios using K-shell α and β lines, such as Cr He_α to Ti He_α, Cr He_β to Ti He_β isoelectronic ratios, Ti or CrLy_α to He_α (or β) interstage ratios, and corresponding ratios using K and Cl. Figure 1(a) compares the density dependences calculated using Ration (at fixed T_e, no radiation field, steady state, and optically thin) of the Cr He_α to Ti He_α isoelectronic and Ti Ly_α to Ti He_α interstage line ratios. Both of the ratios are independent of N_e up to, and somewhat above, the nominal $N_e=10^{21}$ cm^{-3} for which the gas-filled targets in Sec. V, below, were designed. At higher densities, the ionization balance is affected by stepwise electron-collisional excitation. For example, for Ti at $T_e=3$ keV, the electron-collisional ionization rate from the $n=2$ He-like level is 25 times as large as the rate from the ground state. Thus, as density increases, when collisional excitation is sufficient to significantly populate the $n=2$ level, the multistep process consisting of excitation from $n=1$ to 2 (or higher) followed by ionization of the excited state can have a significant contribution. This corresponds to the transition

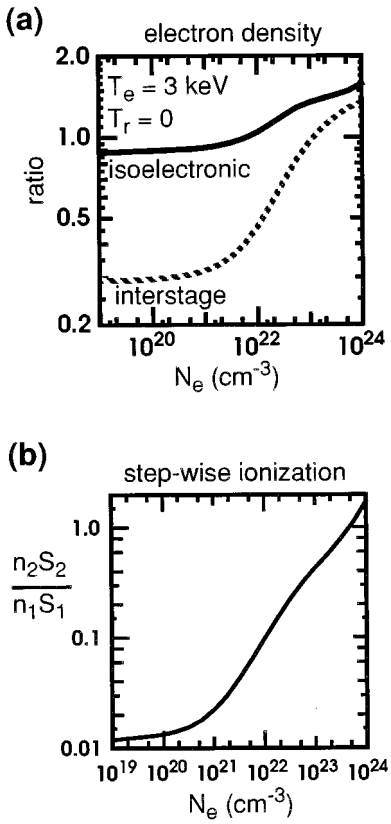

FIG. 1. N_e effects in interstage vs isoelectronic K-shell line ratios. (a) The steady-state Ration model is used to plot the line ratios vs N_e. The ratios are I(Cr He$_\alpha$)/I(Ti He$_\alpha$) (isoelectronic) vs I(Ti Ly$_\alpha$)/I(Ti He$_\alpha$) (interstage). The density dependence, which starts to be significant at densities just below 10^{22} cm^{-3}, is a result of stepwise excitation. (b) The ratio of ionization rates of Ti for the $n=2$ and 1 levels, weighted by the respective level populations.

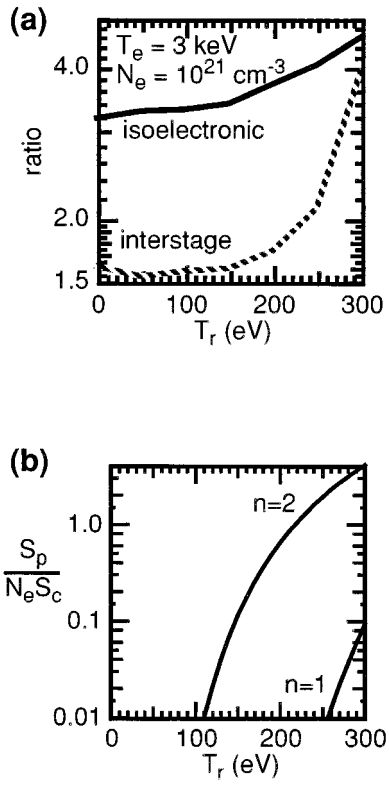

FIG. 2. Radiation-field effects in interstage vs isoelectronic K-shell line ratios. (a) The steady-state Ration model is used to plot the line ratios vs T_r. The ratios are I(K He$_\beta$)/I(Cl He$_\beta$) (isoelectronic) vs I(Cl Ly$_\beta$)/I(Cl He$_\beta$) (interstage). (b) The relative importance of photoionization vs collisional ionization for ionization of the ground and first excited states.

from the coronal to the collisional-radiative regime with increasing N_e. By requiring spontaneous decay to exceed collisional deexcitation for levels up to $n=6$, the limit of the coronal regime is given by [19]

$$N_e < 5.9\times 10^{10} Z^6 T_e^{1/2} \exp\left(\frac{Z^2}{10T_e}\right), \tag{3}$$

where Z is the effective (screened) nuclear charge seen by the transitioning electron, T_e is in eV, and N_e is in cm^{-3}. For He-like Ti at $T_e=3000$ eV, this gives $N_e<2.8\times10^{20}$ cm^{-3}. As an estimate of the relative importance of stepwise ionization of Ti, the quantity n_2S_2/n_1S_1 is plotted against N_e in Fig. 1(b). Here n_2 and n_1 are the populations of the $n=2$ and 1 states and S_2 and S_1 are the respective collisional ionization rates. This was calculated using the Ration model for $T_e=3$ keV. At the higher densities, the fractional change in the interstage ratio is much larger than the change in the isoelectronic line ratio. This occurs because as the He-like stage ionizes with increasing density, a decrease in Ti He$_\alpha$ emission is accompanied by an increase in Ti Ly$_\alpha$ emission, whereas for the isoelectronic case the Cr He$_\alpha$ emission is also decreasing. For the K-Cl case (not shown), the density dependence begins at a slightly lower value of N_e. [Note the Z dependence in Eq. (3) and consider that the K-Cl ratios would be used for lower electron temperature than the Cr-Ti ratios so that the values of Z^2/T_e would be the same in both cases.]

Figure 2(a) shows a similar effect for fixed N_e as the radiation temperature T_r for an imposed Planckian field is increased, this time comparing the I(K He$_\beta$)/I(Cl He$_\beta$) isoelectronic ratio with the I(Cl Ly$_\beta$)/I(Cl He$_\beta$) interstage ratio. In the Nova experiments, it is necessary to use the K-Cl spectra if T_e is much below 2 keV, because emission from Ti and Cr is too weak. Due to the lower Z of K and Cl, the radiation fields are more perturbative and the advantage of the isoelectronic ratio is more significant than for the Cr-Ti scheme. The mechanism for the perturbation by the radiation field is photoexcitation and photoionization from levels $n=2$ and higher. Figure 2(b) plots the ratio of the photoionization rate to the collisional ionization rate vs T_r. For $T_r<300$ eV, the ground state is not significantly perturbed, while the first excited state is affected at $T_r\gtrsim150$ eV. We also find that using a non-Planckian field taken from a LASNEX calculation does not significantly change the results. The non-Planckian field we used was from a LASNEX calculation of a non-gas-filled ''scale-1'' (1600 μm diameter by 2700 μm length) *Hohlraum* target, which is somewhat more energetic than the field for the larger gas-filled *Hohlraum* target discussed in Sec. V B below.

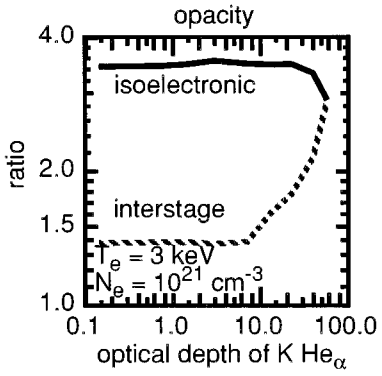

FIG. 3. Opacity effects in interstage vs isoelectronic K-shell line ratios. (a) The steady-state Ration model is used to plot the line ratios I(K He$_\alpha$)/I(Cl He$_\alpha$) (isoelectronic) and I(K Ly$_\alpha$)/I(K He$_\alpha$) (interstage) vs optical depth of the KHe$_\alpha$ line as the escape-factor length is varied.

Figure 3 shows the same kind of effect for opacity, comparing the I(K He$_\alpha$)/I(Cl He$_\alpha$) isoelectronic and I(K Ly$_\alpha$)/I(K He$_\alpha$) interstage ratios. We include the opacity effects using the escape-factor approximation and vary the escape length. The ratios are plotted versus the optical depth of the K He$_\alpha$ line as the escape-factor length is increased. In this situation, the behavior of the interstage ratio depends on the ionization balance as determined by T_e. The populations of $n=2$ levels are perturbed by photoexcitation caused by 2-1 line emission from surrounding ions and the escaping emission depends on the absorption of these same photons, which in turn depends on the ground-state population. In general, there is no simple relation between the opacity effects in the numerator and denominator of the interstage ratio since the ionization balance (ratio between ground-state populations) and hence relative opacities are not necessarily comparable. In the temperature regime where both species in the interstage ratio are abundant, the H-like population increases with rising temperature while the He-like population decreases. Therefore, the opacity of the H-like line would tend to increase with rising temperature while that of the He-like line would decrease. This indicates that the relative importance of opacity for each line is temperature dependent and one could not reasonably hope for a cancellation of opacity effects, even though both lines become more optically thick with increasing escape-factor length. However, in the isoelectronic case, the ground-state populations are comparable over a relatively wide temperature range and the opacity effects tend to cancel as the escape length increases.

Figure 4(a) shows a transient calculation using FLY for a nominal 3-keV model T_e history (simple flat top with a gradual ramp down), with N_e constant at 10^{21} cm^{-3}, comparing the I(Cr He$_\alpha$)/I(Ti He$_\alpha$) isoelectronic and I(Ti Ly$_\alpha$)/I(Ti He$_\alpha$) interstage ratios. The resulting line ratios are then converted back to temperatures assuming steady state, to quantify the transient effects. Neither line ratio agrees perfectly with the model T_e because transient effects cause the ionization balance between He-like and H-like ions to differ from steady-state values. The isoelectronic line ratio more closely follows the changing temperature, particularly during the late recombination phase.

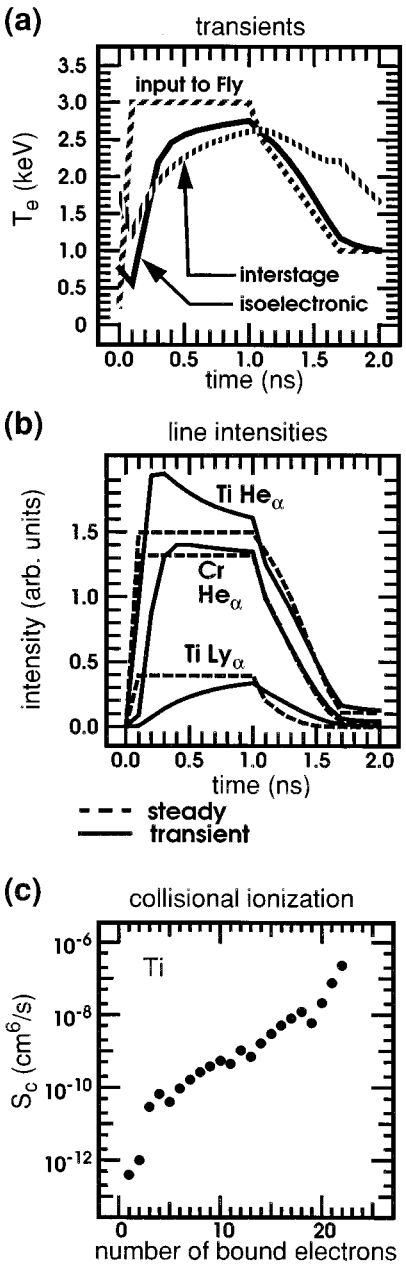

FIG. 4. Transient effects in interstage vs isoelectronic K-shell line ratios. The ratios compared here are the I(Cr He$_\alpha$)/I(Ti He$_\alpha$) isoelectronic and I(Ti Ly$_\alpha$)/I(Ti He$_\alpha$) interstage ratios. The calculations use a model T_e history shown in (a) and assume $N_e=10^{21}$ cm^{-3} and constant in time. (a) uses the FLY code (which contains the Ration model) to perform a transient calculation and uses the resulting line ratios to infer T_e under the invalid assumption of steady state to quantify the transient effects. (b) compares the time behaviors of the individual line intensities to steady state. (c) plots the collisional ionization rates for each ionization stage of Ti vs the number of bound electrons.

Although we find that a partial cancellation of transient effects does occur when the isoelectronic ratio is taken, this is not the primary reason for the superior transient behavior. A more significant effect is that we chose a high enough Z that the H-like population is somewhat less than the He-like population. In this situation, the ionization balance between

He-like and Li-like ions can change rapidly as the temperature changes, while the balance between He-like and H-like ions changes more sluggishly, due to the high ionization potential of the He-like closed-shell configuration. Figure 4(b) plots the raw line intensities vs time for the steady-state and transient calculations. The transient He_α line intensities ''overshoot'' their steady-state values and then gradually approach equilibrium, while the Ly_α line evolves slowly throughout the pulse, never reaching the equilibrium value. Since both He_α lines have the same qualitative transient behavior, there is a partial cancellation in the errors when the ratio is formed, which does not occur for the interstage ratio. However, the isoelectronic ratio is less transient primarily because we used no hydrogenlike lines in the isoelectronic ratio and, for the T_e range that we are considering, the He_α lines are less transient than the Ly_α lines.

Figure 4(c) shows the collisional ionization rates from the Ration model for each ionization stage of Ti plotted vs the number of bound electrons. There is a sudden jump, by a factor of 30, in the curve going from He-like to Li-like ions. Physically, this indicates that the outer $2s$ electron in Li is very weakly bound and thus is easy to ionize. At a density of 10^{21} cm^{-3} and a T_e of 3 keV, a TiCr plasma ionizes quickly to the He-like stage, at which point the He-like population tends to overaccumulate (more than steady state) until final equilibrium with the H-like and fully stripped stages occurs on a longer time scale. For the parameters in Fig. 4, relatively little H-like population is produced, as evidenced by the relatively weak Ti Ly_α intensity. In this case, the He-like ionization dynamics are dominated by the ionization balance with Li-like ions. If a lower Z were chosen for the spectral dopants, the transient effects for heliumlike lines would be greater at this temperature. If a higher Z were chosen, the transient effects would be reduced further, but the He-like line emission intensity would decrease due to the reduced excitation from the ground state. Thus the choice of Z represents a compromise between considerations of transient effects and limitations due to sensitivity of the diagnostic instrumentation and the ability to discriminate signal from background emission.

Not surprisingly, if there is a significant temperature gradient in the emitting region, LASNEX-DSP calculations show that the emissions from the isoelectronic states are peaked at approximately the same spatial locations, whereas the interstage emissions can come from different locations and thereby sample different temperatures. We thus have more confidence that the temperature deduced from an isoelectronic ratio would be representative of the temperatures in the emitting region when there are gradients.

IV. ANALYTIC TREATMENT OF MODELING UNCERTAINTIES

Since Marjoribanks *et al.* [7] have stated that modeling uncertainties tend to cancel when isoelectronic line ratios are formed, one might hope that a simple analytic model would produce approximately the same line ratios as Ration. We have found that a very simplified analytic treatment can yield results roughly comparable to the full Ration model. Calculations using the analytic formulas exhibit reduced sensitivity to uncertainty in dielectronic recombination, which is important for reasons discussed in the following paragraph. We do not feel that the analytic treatment presented below yields results sufficiently accurate for data analysis, but it does demonstrate explicitly the manners in which the isoelectronic ratios have reduced sensitivity to modeling uncertainty. We suspect that, with more work, the model could be improved to yield accurate quantitative predictions, but that would be beyond the scope of the present work.

In this section, we present a simple model containing only two ionization stages, each of which has only a ground state and a single excited state. The kinetics is assumed to be coronal equilibrium except that dielectronic recombination is included as coupling the ground state of one ion stage to the ground state of the other stage. By assuming coronal kinetics, we are limiting this model to plasmas whose electron densities are below the limit given approximately by Eq. (3). This limitation could be relaxed by including multistep ionization and perhaps other processes (such as three-body recombination), at the expense of significant added complexity. Dielectronic recombination is of concern because its treatment in Ration is very simplified. In general, accurate treatment of dielectronic recombination requires a model with many multiply excited states. But the only multiply excited states included in Ration are doubly excited heliumlike and lithiumlike states with both excited electrons in $n=2$ levels. This approximation might be acceptable at relatively low quasicoronal densities, such as we are considering, but would be more questionable at higher densities where there are more electrons in excited states. The dielectronic-recombination model we use in our analytic treatment is even more simplified. In particular, the dielectric recombination model we use introduces a coupling between the ground states of the two ionization stages, but does not include any direct rates into or out of the excited states.

This analytic model is also a steady-state model. It would not be difficult to add time dependence to this model. One can see some examples of how modeling uncertainties cancel out in the derivation of the model, and the insensitivity to modeling variation will be demonstrated by comparing the results with the full Ration model and by turning off the dielectronic recombination in the analytic model.

For the densities and temperatures typical of subcritical Nova plasmas, we find that the dominant atomic kinetic rates are electron collisional ionization, radiative recombination, electron collisional excitation, and spontaneous decay. Dielectronic recombination is also a significant effect. The collisional ionization rate is taken from Lotz [10–12]:

$$S=\left(\frac{8}{\pi m_e}\right)^{1/2}\frac{a\xi}{P\sqrt{T_e}}E_1(U), \tag{4}$$

where S is the collisional ionization rate for a particular ionization stage, m_e is the electron mass, $a=4.4379\times10^{-14}$ eV^2 cm^2, ξ is the number of bound electrons in the outer subshell of the initial ionization stage, P is the ionization potential of initial ionization stage, T_e is the electron temperature, $U=P/T_e$, and E_1 is the exponential integral of the first kind.

Spontaneous radiative recombination is from Spitzer [20] (and is equivalent to the treatment of Seaton [21] with the Gaunt factor equal to 1):

$$R=\frac{2^6\sqrt{\pi}}{3^{3/2}}r_e^2cZU^{3/2}\exp(U)E_1(U), \tag{5}$$

where R is the spontaneous radiative recombination rate for a particular initial ionization stage, r_e is the classical electron radius, c is the speed of light, and Z is the charge on the initial ionization stage including inner-electron screening. Collisional excitation is from Van Regemorter [22] (with the Gaunt factor=0.2):

$$C=(\pi a_0^2)E_R^2\left(\frac{2}{3\pi m_e}\right)^{1/2}\frac{16\pi}{5}\frac{\exp(-\Delta E/T_e)}{\Delta E\sqrt{T_e}}f, \tag{6}$$

where C is the collisional excitation rate from initial to final level of a particular ion, a_0 is the Bohr radius, E_R is the Rydberg energy (13.606 eV), ΔE is the energy of transition from initial to final level, and f is the oscillator strength of the transition. The oscillator strength is a dimensionless measure of the spontaneous decay rate and is related to it by

$$A=\frac{2c}{a_0}\left(\frac{\Delta E}{m_ec^2}\right)^2\frac{g_l}{g_u}f, \tag{7}$$

where A is the spontaneous transition rate from upper to lower level and g_l, g_u are the statistical weights of lower and upper states.

These expressions for S, R, C, and A are the same as in the Ration model, but we treat dielectronic recombination using the analytic fit for the total dielectric recombination rate obtained by Burgess [23,24]:

$$D=\frac{7.589\times10^{-14}}{T_e^{3/2}}f\alpha(x)\beta(Z)\exp\left[\frac{-x\gamma(Z)}{T_e}\right]\delta(Z)\ \ \mathrm{cm^3/s}, \tag{8}$$

where

$$x=\frac{\Delta E}{E_R(1+Z)},$$

$$\alpha(x)=\frac{\sqrt{x}}{1+0.105x+0.015x^2},$$

$$\beta(Z)=\left(\frac{Z(1+Z)^5}{Z^2+13.4}\right)^{1/2}, \tag{9}$$

$$\gamma(Z)=\left(\frac{1}{73.44}\right)\frac{1+Z}{1+\dfrac{0.015Z^3}{(1+Z)^2}},$$

$$\delta(Z)=0.84+\frac{0.5}{(1+Z^2)}+\frac{0.03(Z-11)}{1+4.5\times10^{-5}(Z-11)^3}.$$

In this form of the Burgess formula, T_e is in keV. The other rate formulas are valid in any self-consistent system of units with T_e in energy units.

As another simplification compared to Ration, we use a simple hydrogenic formula for the transition energies from excited to ground states:

$$E(n,Z)=P(Z)\left(1-\frac{1}{n^2}\right), \tag{10}$$

where E is the energy of excitation level n, n is the principal quantum number, Z is the screened nuclear charge, and the ionization potential is given by

$$P(Z)=Z^2E_R. \tag{11}$$

In this analysis, with the exception of the dielectronic recombination term, the oscillator strength will only appear as the ratio $f_{n\mathrm{H}}/f_{n\mathrm{He}}$ of an n-to-1 transition in the hydrogenic species to the corresponding transition in the heliumlike ion. In this case, it is a fairly good approximation to take

$$\frac{f_{2\mathrm{H}}}{f_{2\mathrm{He}}}=1.5. \tag{12}$$

We consider a simplified system of only two ionization stages and two levels, described by the following four dependent variables: N_{H}, the population of hydrogenic ground state; N_{He}, the population of heliumlike ground state; Y, the population of hydrogenic excited state; and X, the population of heliumlike excited state. These variables are related by three rate equations and by conservation of particles. The steady-state ionization balance equation is

$$0=N_eRN_{\mathrm{H}}-N_eSN_{\mathrm{He}}+N_eDN_{\mathrm{H}}, \tag{13}$$

the excitation balance equation for hydrogen is

$$0=N_eC_{\mathrm{H}}N_{\mathrm{H}}-A_{\mathrm{H}}Y, \tag{14}$$

and the excitation balance equation for helium is

$$0=N_eC_{\mathrm{He}}N_{\mathrm{He}}-A_{\mathrm{He}}X, \tag{15}$$

where we assume that dielectronic recombination couples the hydrogenic ground state to the heliumlike ground state, which is consistent with the Burgess formulation. (A more careful treatment would split the process into a recombination into the excited state followed by a competition between autoionization and spontaneous decay.) We also assume that $X, Y \ll N_{\mathrm{He}}, N_{\mathrm{H}}$ so that the conservation equation is simply

$$N_{\mathrm{H}}+N_{\mathrm{He}}=N, \tag{16}$$

where N is the total number of ions present. The subscripts on C indicate that C is a function of which ionization stage is being excited. Solving for the excited-state populations yields

$$X=N_eNK_{\mathrm{He}}\frac{1+F}{1+I+F} \tag{17}$$

and

$$Y=N_eNK_{\mathrm{H}}\frac{I}{1+I+F}, \tag{18}$$

where

$$I=\frac{S}{R}=\frac{3614.5}{P\sqrt{T_e}ZU^{3/2}\exp(U)}, \tag{19}$$

$$K=\frac{C}{A}=2.305\times10^{-24}\frac{\exp(-\Delta E/T_e)}{(\Delta E)^3\sqrt{T_e}}\ \text{cm}^3, \tag{20}$$

$$F=\frac{D}{R}=\frac{1.4603}{P^{3/2}\exp(U)E_1(U)}f\alpha(x)\beta(Z)\times\exp\left[\frac{-x\gamma(Z)}{T_e}\right]\delta(Z)\ \text{cm}^3, \tag{21}$$

with N_e in cm^{-3} and T_e in keV. Note that, due to cancellations, the oscillator strength appears only in the expression F, which represents dielectronic recombination.

The intensities (L_{He} and L_{H}, respectively) of emission lines for n-to-1 transitions of heliumlike and hydrogenlike ionization stages are now given by

$$L_{\text{He},n}(Z,T_e)=X_n(Z,T_e)\Delta E_{\text{He},n}(Z)A_{\text{He},n}(Z) \tag{22}$$

and

$$L_{\text{H},n}(Z,T_e)=Y_n(Z,T_e)\Delta E_{\text{H},n}(Z)A_{\text{H},n}(Z). \tag{23}$$

At this point, when one forms the isoelectronic line ratio $L_{\text{He}}(Z+\Delta Z)/L_{\text{He}}(Z)$, one can see, for example, that the effects of dielectronic recombination enter the numerator and denominator in the same way, which does not happen for an interstage line ratio such as $L_{\text{H}}(Z)/L_{\text{He}}(Z)$. Moreover, the oscillator strength, which appears in A, cancels when the isoelectronic intensity ratio is formed, to the extent that $f(Z)\cong f(Z+\Delta Z)$. This does not occur in the interstage line ratio, where the ratio $f_{\text{H}}(Z)/f_{\text{He}}(Z)$ appears, for which we use Eq. (12).

This cancellation of the dependence on oscillator strengths is very convenient and illustrates how a particular physical effect cancels when forming the ratio. However, this alone is not necessarily an advantage for isoelectronic ratios because, although to our knowledge oscillator strengths for the resonance lines of the elements we consider have not been measured experimentally, calculational techniques for them have been well bench-marked. The demonstration of reduced sensitivity to uncertainty in dielectronic recombination is perhaps more interesting. Although in principle dielectronic recombination can be accurately modeled, it generally requires a much more complete set of multiply excited states than is included in the Ration model. We illustrate the reduced sensitivity to dielectronic recombination by comparing calculations using the analytic model with the results from Ration calculations using both the interstage and isoelectronic ratios.

Figure 5 compares the analytic model with Ration for isoelectronic and interstage ratios, with and without dielectronic recombination (DR). The relative insensitivity of the isoelectronic ratio to modeling differences is easy to see. In Fig. 5(a) the analytic model for the isoelectronic ratio agrees fairly well with the full Ration model, considering the simplicity of the analytic model. The departure from Ration as temperature increases is probably due to either the neglect of the fully stripped ionization stage or to the neglect of the coupling to the excited state by dielectronic recombination, or both. (One could add a fully stripped stage to the analytic model fairly easily, but a better analytic treatment of DR would require a Burgess-like model that has separate recombination rates for coupling to the ground and excited states.) The very close agreement for the isoelectronic ratio when DR is not included is probably a coincidence, as the Ration model has a better treatment of DR than the analytic model. The main point of Fig. 5 is that the both the departures from

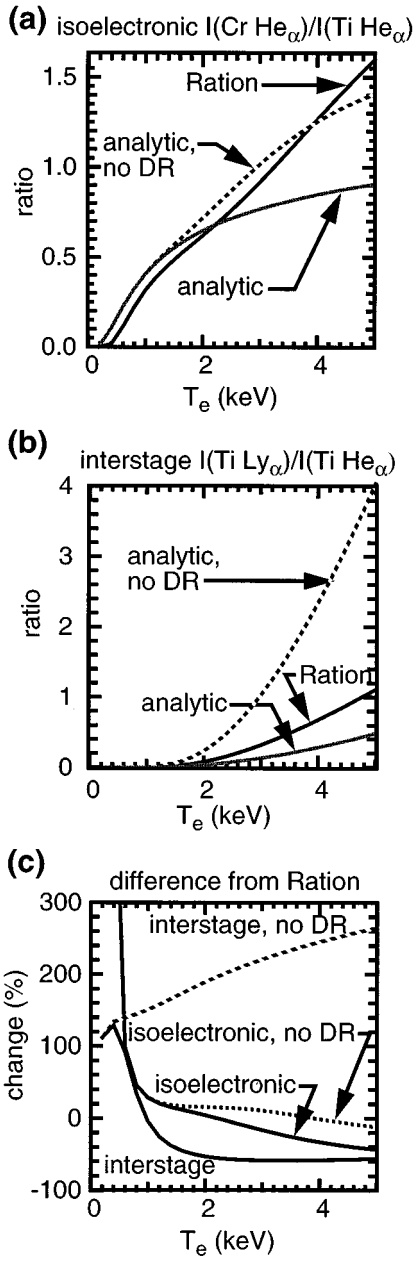

FIG. 5. Comparison of simple analytic and full Ration models. (a) The analytic isoelectronic ratio $I(\text{Cr He}_\alpha)/I(\text{Ti He}_\alpha)$ with and without dielectronic recombination (DR) and the full Ration model vs T_e. (b) The same comparison for the interstage ratio $I(\text{Ti Ly}_\alpha)/I(\text{Ti He}_\alpha)$. (c) The percentage ''error'' compared to the full Ration model. The analytic model is explicitly independent of N_e and T_r and the Ration calculation used $N_e=10^{21}\ \text{cm}^{-3}$ and $T_r=0$.

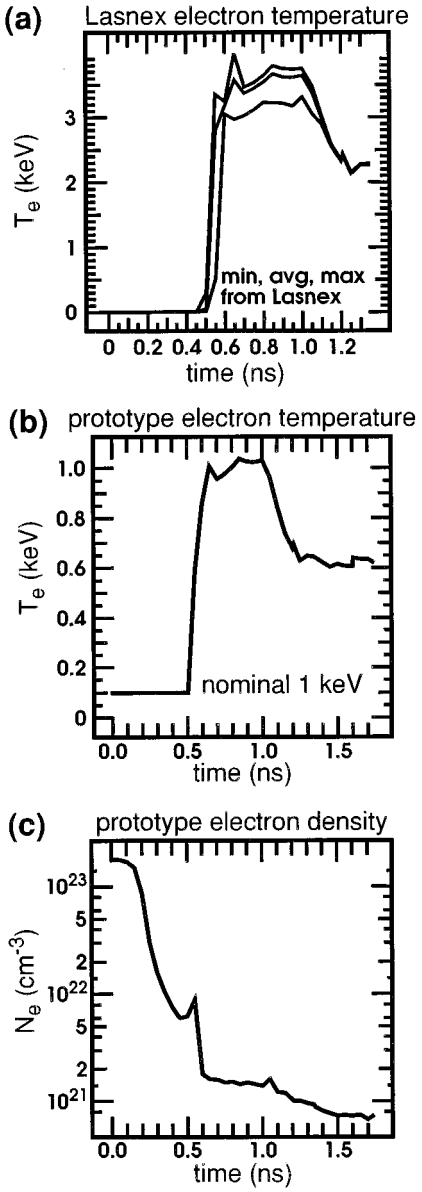

FIG. 6. Prototype temperature and density from Lasnex gas-bag calculation. (a) The minimum, average, and maximum T_e in the directly illuminated portion of the fiber vs time; (b) a scaled prototypical temperature history; and (c) the prototypical density history.

Ration and the effect of omitting DR are smaller for the isoelectronic line ratio than for the interstage ratio. For the interstage ratio in Fig. 5(b) the analytic model departs markedly from Ration, and omitting DR changes the results dramatically. Figure 5(c) shows that the relative error in the analytic model compared to Ration is much greater for the interstage ratio than for the isoelectronic ratio. [Note that at low temperatures (below 0.8 keV), where significant lithiumlike ionization stage is expected, the analytic result gives inaccurate results even for the isoelectronic ratio. This is not surprising since the lithiumlike stage is not included in the model. In an experimental application, it is unlikely that heliumlike and hydrogenic lines would be observable in this temperature range.]

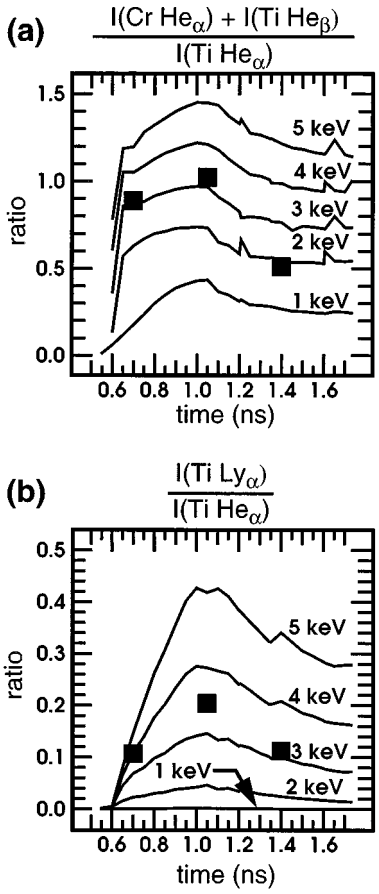

FIG. 7. LASNEX-FLY analysis for the gas bag. The prototypical line ratio histories corresponding to each nominal T_e history are shown for (a) the isoelectronic line ratio and (b) the interstage line ratio. Experimental data points are shown as rectangles.

V. APPLICATION TO EXPERIMENTAL DATA

In this section, we briefly illustrate the application of isoelectronic-line-ratio techniques to infer experimental electron temperatures for gas bags and gas-filled *Hohlraum* targets. Further experimental details can be found in the related experimental papers [25–27].

We used FLY and DSP calculations to infer T_e from experimental data: FLY for quick analysis and DSP to more accurately fold in the spatial variations. For input to FLY, we spatially averaged LASNEX hydrodynamics data to obtain zero-dimensional time histories of density and temperature of the emitting region. Scaled temperatures were used to perform several FLY calculations to yield a family of line ratios vs time with ''nominal'' T_e as a parameter. These data were compared with experimental data to infer the actual temperature.

We input two-dimensional (2D) LASNEX data into DSP. DSP calculates spectral emissivity and opacity for each spatial zone, integrates line-transfer equations along lines of sight, and performs appropriately weighted sums to simulate the spectrum from the experimental diagnostic. After convolving with an instrument function, we compared the calculated spectrum with the experimental data.

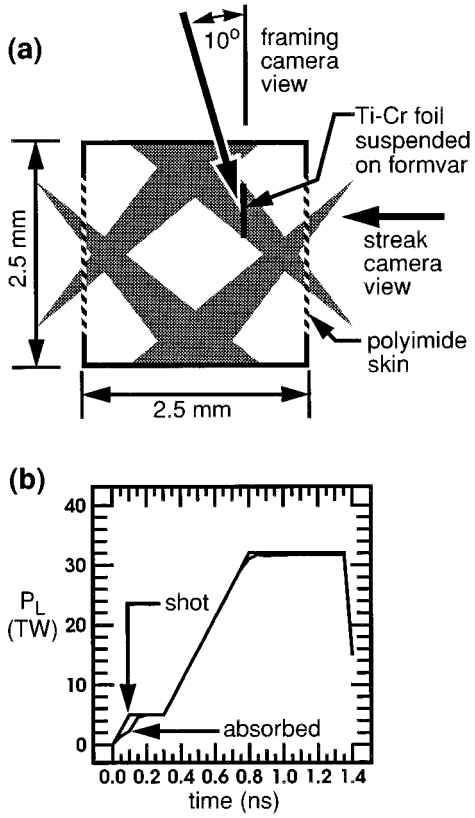

FIG. 8. Gas-filled *Hohlraum* target design. The geometry of the target shown in (a) is cylindrically symmetric about the horizontal axis. The target is illuminated with 30 kJ of 0.35-μm light with the pulse shape shown in (b) from the LASNEX calculation. The two curves marked ''shot'' and ''absorbed'' are the incident and the absorbed laser power, respectively. The absorption model in LASNEX predicts that most of the incident energy is absorbed.

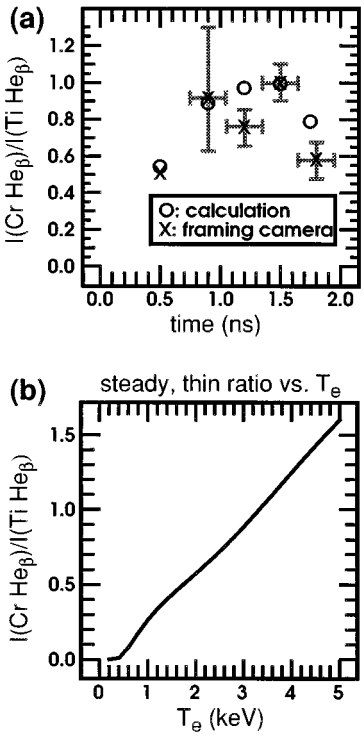

FIG. 9. LASNEX-DSP analysis for the gas-filled *Hohlraum* target. (a) compares the calculated ratios for the $I(\mathrm{Cr\ He}_\beta)/I(\mathrm{Ti\ He}_\beta)$ isoelectronic line ratio with data from a framing camera. (b) shows the dependence of the line ratio on T_e in the steady-state approximation. The predicted temperature from LASNEX is about 25% higher than one would infer from (b) due to transient effects that are included in the calculation in (a).

A. Gas-bag measurements

Figures 6 and 7 illustrate the relatively quick LASNEX-FLY analysis technique using data from Nova gas-bag experiments [25,26]. Figure 6 shows hydrodynamics data from a LASNEX gas-bag simulation. The target is a 3-mm-diam spherical bag made of 5000-Å-thick polyimide and pressurized at 1 atm with neopentane (C_5H_{12}). The target is illuminated with 27 kJ of 0.35-μm light from 10 Nova beams in a 1-ns square pulse. Suspended along the vertical axis of the bag is a 9-μm-diam C fiber coated with a 2000-Å-thick TiCr alloy. We measured the atomic ratio of Ti to Cr in the surface layer on the fiber using x-ray fluorescence. It takes 0.5 ns for the laser to ionize the surrounding gas and reach the fiber at the center of the gas bag. The TiCr surface layer on the fiber then heats rapidly to over 3 keV. We took prototype temperatures and densities from LASNEX by averaging the central 1-mm portion of the fiber length and performed FLY calculations for nominal ''flat-top'' T_e values ranging from 1 to 5 keV [Figure 6(b) shows the nominal $T_e=1$ keV temperature history.] For numerical reasons, a constant 100-eV foot was added to each prototypical T_e history.

Figure 7 shows the resulting line ratios, for each scaled prototypical T_e history, with experimental data [26] superimposed. Due to the limited spectral resolution of the spectrometer, closely spaced lines tended to blend together. To model these blended lines, we calculated the individual intensities of each of the component lines and summed them together before forming the ratios. The isoelectronic and interstage line ratios are consistent with a T_e history slightly hotter than the nominal 3-keV case, in close agreement with the LASNEX hydrodynamics data. There is also evidence that the temperature decreases more rapidly after the end of the laser pulse than LASNEX predicts.

B. Gas-filled *Hohlraum* measurements

Figures 8 and 9 illustrate the LASNEX-DSP analysis technique using data from Nova gas-filled *Hohlraum* experiments [27]. We modeled a gas-filled *Hohlraum* containing a TiCr diagnostic foil using LASNEX and postprocessed with DSP. Figure 8(a) shows the target, consisting of a hollow Au cylinder pressurized with 1-atm neopentane (C_5H_{12}). It is illuminated with 30 kJ of 0.35-μm light in 10 Nova beams with the pulse shape shown in Fig. 8(b). A 2000-Å-thick, 100-μm-wide TiCr diagnostic foil is suspended on an 800-Å-thick formvar film at the position shown. A spectrometer mounted on a framing camera views through a hole in the Au wall and a streaked spectrometer views through the laser entrance hole.

Figure 9 shows the results of the LASNEX-DSP analysis. We used the $I(\mathrm{Cr\ He}^{\mathrm{gb}})/I(\mathrm{Ti\ He}_\beta)$ ratio as a T_e diagnostic,

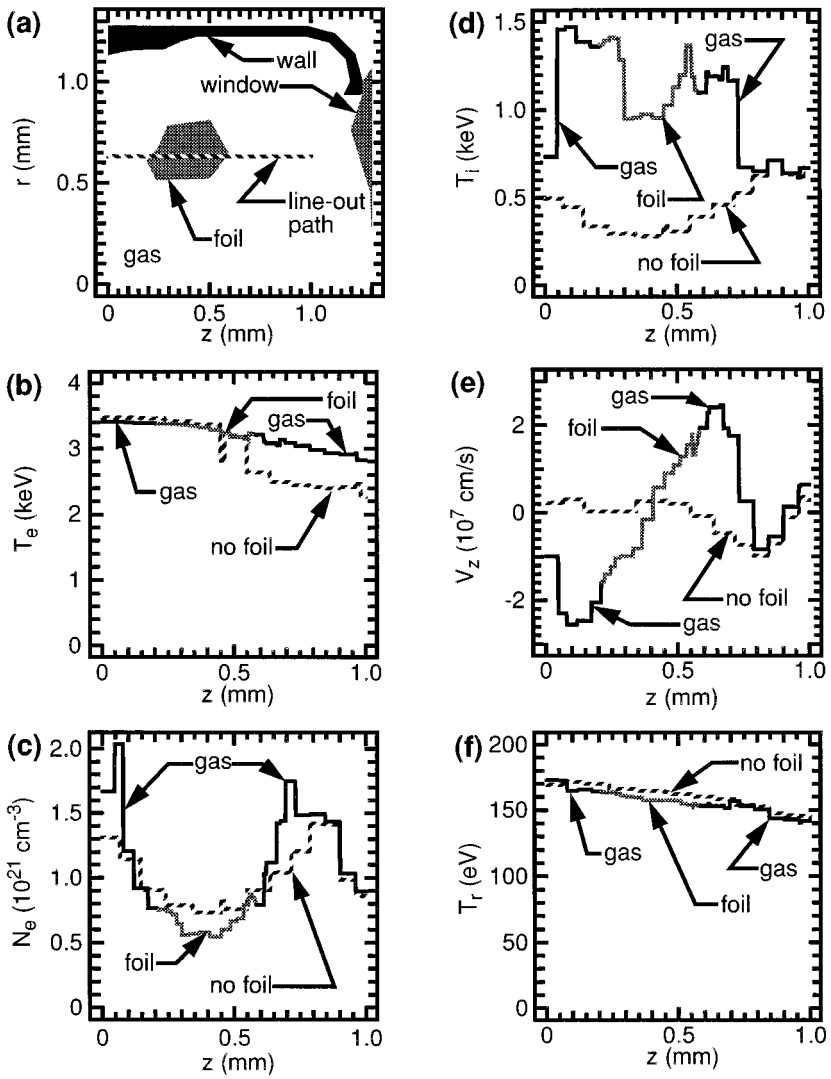

FIG. 10. LASNEX calculations compared with vs without diagnostic foil. (a) shows the problem geometry at 1 ns and assumes cylindrical symmetry about the z axis and reflection symmetry about the $z=0$ plane. Quantities plotted along the line-out path shown are T_e in (b), N_e in (c), T_i in (d), T_r in (e), and fluid velocity in the z direction (V_z) in (f).

which exhibits close agreement between experiment and calculation. The spatial average of the LASNEX T_e data for the TiCr foil (182 zones) reaches a peak at 3.7 keV, which is about 25% higher than one would infer from the steady-state approximation shown in Fig. 9(b). This is due to transient effects that were included in the Fig. 9(a) calculation. Transients cause both line ratios to lag behind the steady-state values, which would result in an underestimate of the temperature if transients were ignored in the data analysis. This underestimate would be more severe in the case where one used the interstage line ratio.

VI. PERTURBATIONS FROM THE FIBERS AND FOILS

To evaluate the extent to which the plasma is perturbed by these measurements, we repeated the LASNEX gas-bag and *Hohlraum* calculations without the diagnostic fiber or foil. The presence of solid material that must ablate causes perturbations in N_e and flow velocity. The increase in laser absorption and collisional coupling between electrons and ions, due to the higher Z of the Ti and Cr, causes increases in electron and ion temperature. Shocks that are launched in the fiber or foil also heat the ions.

Figure 10 compares the results from two LASNEX calculations, which were identical except that the diagnostic foil was included in one case and omitted in the other. The data in Fig. 10 were taken at time $t=1.0$ ns from the beginning of the laser pulse. Figure 10(a) shows the configuration of one quadrant of the *Hohlraum* target at 1 ns. The foil material in the calculation was initially placed in the path of the laser. The thickness of the foil was the same as in the experiment, but the radial extent of the foil was chosen so that the foil contained the same mass as in the experiment. This was necessary to avoid significantly over-estimating the perturbing effects, since the experiment had only a thin strip of foil while a 2D calculation would model this as a full disk (or ring) of foil. The data in Figs. 10(f)–10(b) are plotted along the line-out path shown in Fig. 10(a). The laser is incident from the right.

The T_e perturbation shown in Fig. 10(b) is insignificant. The temperature of the gas region to the right of the foil is slightly higher when the foil is present because some laser energy is reflected back toward this region early in the pulse before the laser burns through the foil. The N_e perturbation in Fig. 10(c) is also insignificant, particularly since the line ratios used in the analysis have very weak density dependence for these densities. The perturbations in N_e and T_e are larger earlier in the calculation, but the emission from the spectral dopants is too weak to detect experimentally at early

time, and we are primarily interested in the temperature during the flat top of the pulse for related plasma instability studies. In fact, the higher density during ablation of the fiber or foil is beneficial because it accelerates the ionization transient by temporarily enhancing the collisional ionization rate. We have seen this by comparing FLY calculations, which assume N_e to be constant at 10^{21} cm^{-3} with calculations using density and corresponding temperature histories taken from LASNEX calculations.

The ion temperature and velocity gradient perturbations shown in Figs. 10(d) and 10(e) reduce the optical depth of the lines, which is usually of no consequence to the measurement if the experiment is designed to produce optically thin lines. Figure 10(f) shows that there is almost no perturbation in T_r produced by the foil. This is important because, although the diagnostic itself has weak T_r dependence, a significant perturbation in T_r would affect the radiative ablation physics, which is generally undesirable.

VII. CONCLUSION

Isoelectronic line ratios, which are formed using the same line from two elements of slightly different atomic numbers, are good temperature diagnostics for *Hohlraum* plasmas due to reduced sensitivity to electron density, radiation field, opacity, transients, and spatial gradients compared with conventional ratios. This insensitivity reduces the uncertainty that is introduced when nonideal effects are treated in the modeling and increases our confidence in the accuracy of our analysis. By comparing our modeling results with experimental data, we find that the Nova gas bags and gas-filled *Hohlraum* targets have electron temperatures of at least 3 keV.

ACKNOWLEDGMENTS

We wish to thank R. W. Lee for providing the Ration and FLY computer codes, Hans Griem for many enlightening discussions on physics issues, and the LLNL and Los Alamos National Laboratory Target Fabrication groups for construction of the gas-filled targets used in the experiments. We also thank M. D. Rosen for support and encouragement and for bringing the work of R. S. Marjoribanks on isoelectronic line ratios to our attention. This work was performed under the auspices of the U.S. Department of Energy by Lawrence Livermore National Laboratory under Contract No. W-7405-Eng-48.

[1] R. Kauffman, in *Handbook of Plasma Physics, Vol. 3: Physics of Laser Plasma*, edited by A. M. Rubenchik and S. Witkowski (Elsevier, Amsterdam, 1991), pp. 111–162.
[2] H. A. Baldis, E. M. Campbell, and W. L. Kruer, in *Handbook of Plasma Physics, Vol 3: Physics of Laser Plasma* (Ref. [1]), pp. 361–434.
[3] R. L. Kauffman, L. J. Suter, C. B. Darrow, J. D. Kilkenny, H. N. Kornblum, D. S. Montgomery, D. W. Phillion, M. D. Rosen, A. R. Theissen, R. J. Wallace, and F. Ze, Phys. Rev. Lett. **73**, 2320 (1994).
[4] J. Abdallah, Jr., R. E. H. Clark, C. J. Keane, T. D. Shepard, and L. J. Suter, J. Quant. Spectrosc. Radiat. Transfer **50**, 91 (1993).
[5] T. D. Shepard, C. J. Keane, L. J. Suter, and J. Abdallah, Jr., Rev. Sci. Instrum. **63**, 5101 (1992).
[6] T. R. Dittrich, B. A. Hammel, C. J. Keane, R. McEachern, R. E. Turner, S. W. Haan, and L. J. Suter, Phys. Rev. Lett. **73**, 2324 (1994).
[7] R. S. Marjoribanks, M. C. Richardson, P. A. Jaanimagi, and R. Epstein, Phys. Rev. A **46**, R1747 (1992).
[8] R. W. Lee, B. L. Whitten, and R. E. Stout, J. Quant. Spectrosc. Radiat. Transfer **32**, 91 (1984).
[9] R. W. Lee, *User Manual for Ration* (Lawrence Livermore National Laboratory, Livermore, 1990).
[10] W. Lotz, Z. Phys. **206**, 205 (1967).
[11] W. Lotz, Z. Phys. **216**, 241 (1968).
[12] W. Lotz, Z. Phys. **220**, 486 (1969).
[13] C. J. Keane, R. W. Lee, and J. P. Grandy, in *Radiative Properties of Hot Dense Matter*, Proceedings of the Fourth International Workshop, 1990, Sarasota, edited by W. Goldstein, C. Hooper, J. Gauthier, J. Seely, and R. Lee (World Scientific, River Edge, NJ, 1991), pp. 233–241.
[14] G. B. Zimmerman and W. L. Kruer, Comments Plasma Phys. **2**, 51 (1975).
[15] An early, steady-state version of the code written by R. W. Lee was called Ration. We use the expression ''Ration model'' to refer to the kinetics model from this code when it is implemented in the newer codes FLY and DSP.
[16] J. P. Apruzese, J. Davis, D. Duston, and K. G. Whitney, J. Quant. Spectrosc. Radiat. Transfer **23**, 479 (1980).
[17] J. P. Apruzese, J. Quant. Spectrosc. Radiat. Transfer **25**, 491 (1981).
[18] We use the expression ''interstage line ratio'' to refer generically to a line ratio between corresponding transitions in adjacent ionization stages [e.g., $(\mathrm{Ly}_\alpha)/(\mathrm{He}_\alpha)$].
[19] C. DeMichelis and M. Mattioli, Nucl. Fusion **21**, 677 (1981).
[20] L. Spitzer, Jr., Astrophys. J. **107**, 6 (1948).
[21] M. J. Seaton, Mon. Not. R. Astron. Soc. **119**, 81 (1959).
[22] H. Van Regemorter, Astrophys. J. **136**, 906 (1962).
[23] A. Burgess, Astrophys. J. **139**, 776 (1964).
[24] A. Burgess and A. S. Tworkowski, Astrophys. J. **205**, L105 (1976).
[25] D. H. Kalantar, D. E. Klem, B. J. MacGowan, J. D. Moody, D. S. Montgomery, D. H. Munro, T. D. Shepard, G. F. Stone, B. H. Failor, and W. W. Hsing, Phys. Plasmas **2**, 3161 (1995).
[26] B. H. Failor, W. W. Hsing, R. G. Hockaday, T. D. Shepard, D. E. Klem, D. H. Kalantar, and B. J. MacGowan, Rev. Sci. Instrum. **66**, 767 (1995).
[27] L. V. Powers, R. E. Turner, R. L. Kauffman, R. L. Berger, P. Amendt, C. A. Back, T. P. Bernat, S. N. Dixit, D. Eimerl, J. A. Harte, M. A. Henesian, D. H. Kalantar, B. F. Lasinski, B. J. MacGowan, D. S. Montgomery, D. H. Munro, D. M. Pennington, T. D. Shepard, G. F. Stone, L. J. Suter, and E. A. Williams, Phys. Rev. Lett. **74**, 2957 (1995).